HOKKAIDO UNIVERSITY

Title	Synthesis and preclinical evaluation of a 68Ga-labeled peptide for PET imaging of transferrin receptor 1 in tumor
Author(s)	Lin, Longxin; Mizuno, Yuki; Shibata, Yuki et al.
Citation	European Journal of Nuclear Medicine and Molecular Imaging, 53(1), 687-696 https://doi.org/10.1007/s00259-025-07493-8
Issue Date	2025-08-08
Doc URL	https://hdl.handle.net/2115/98009
Rights	This version of the article has been accepted for publication, after peer review (when applicable) and is subject to Springer Nature's AM terms of use, but is not the Version of Record and does not reflect post-acceptance improvements, or any corrections. The Version of Record is available online at: http://dx.doi.org/10.1007/s00259-025-07493-8
Type	journal article
File Information	Main Text.pdf

Hokkaido University Collection of Scholarly and Academic Papers : HUSCAP

Synthesis and Preclinical Evaluation of a ^{68}Ga-Labeled Peptide for PET Imaging of Transferrin Receptor 1 in Tumor

Longxin Lin[1], Yuki Mizuno[2,3]*, Yuki Shibata[2], Hironobu Yasui[4], Yuji Kuge[2,3]

[1] **Graduate School of Biomedical Science and Engineering, Hokkaido University, Hokkaido 060-0815, Japan.**

[2] **Central Institute of Isotope Science, Hokkaido University, Hokkaido 060-0815, Japan.**

[3] **Global Center for Biomedical Science and Engineering, Hokkaido University, Hokkaido 060-0815, Japan.**

[4] **Faculty of Veterinary Medicine, Hokkaido University, Hokkaido 060-0818, Japan**

***Corresponding author at: Central Institute of Isotope Science, Hokkaido University, Hokkaido 060-0815, Japan.**

Email address: mizuno@ric.hokudai.ac.jp (Y. Mizuno)

Abstract (150-250 words)

Purpose:

Transferrin receptor 1 (TfR1) is a transmembrane glycoprotein that mediates cellular iron uptake. Despite its potential as a target for tumor diagnosis, the lack of suitable TfR1 ligands has hindered the development of effective TfR1 imaging agents. We labeled a recently discovered TfR1 ligand, TfRB1G3, with Ga-68 and evaluated its potential for TfR1 imaging through preclinical experiments.

Methods:

TfRB1G3 was modified with HBED-CC and radiolabeled with $^{67/68}$Ga ([$^{67/68}$Ga]Ga-TfRB1G3). Human glioblastoma (U87MG) cells were transfected with TfR1-targeting siRNA (TfR1-knockdown) or non-targeting siRNA (control), and accumulation of [^{67}Ga]Ga-TfRB1G3 was evaluated. The K_D value of [^{67}Ga]Ga-TfRB1G3 for TfR1 was also calculated. Ex vivo biodistribution was conducted in normal and U87MG tumor-bearing mice after injecting [^{67}Ga]Ga-TfRB1G3. PET imaging studies were conducted after injecting [^{68}Ga]Ga-TfRB1G3, with/without co-injection of 10 nmol TfRB1G3 in mice bearing U87MG tumors.

Results:

[$^{67/68}$Ga]Ga-TfRB1G3 was obtained with high radiochemical purity (> 90%). The accumulation of [^{67}Ga]Ga-TfRB1G3 in the TfR1-knockdown cells (22.0 ± 1.1% Dose/mg) was significantly lower than that in the control (308.5 ± 14.3% Dose/mg). The K_D value was 1.0 nM. Tumor accumulation of [^{67}Ga]Ga-TfRB1G3 was higher than in any other organs except the kidneys, and co-injection of TfRB1G3 significantly reduced the tumor accumulation by more than 90%. PET imaging with [^{68}Ga]Ga-TfRB1G3 clearly visualized TfR1-positive tumor as early as 20 min post-injection.

Conclusion:

[^{68}Ga]Ga-TfRB1G3 demonstrated excellent affinity and specificity for TfR1 both in vitro and in vivo, providing clear PET images of TfR1-positive tumors shortly after injection. [^{68}Ga]Ga-TfRB1G3 would enable sensitive and quantitative imaging of TfR1 expression.

Key Words: Positron emission tomography (PET); Gallium-68 (^{68}Ga); Transferrin receptor (TfR); Cysteine-dense peptide

Introduction

Transferrin receptor 1 (TfR1, also known as CD71) is a type II transmembrane glycoprotein found as a homodimer on the cell membrane and mediates the uptake of holo-transferrin (diferric transferrin), which is the main iron transport protein in blood plasma, into cells. Thus, TfR1 plays an essential role in regulating iron import as part of cellular iron metabolism [1, 2]. Furthermore, according to the MERAV database [3], the Human Protein Atlas database [4], and other studies [5, 6], TfR1 expression is specifically upregulated in various tumor types, including glioma, prostate cancer, and breast cancer. In addition, the TfR1 expression level is associated with aggravated proliferation, migration, invasion, apoptosis, and metastasis of tumors [7-10]. Therefore, TfR1 is a promising target for both nuclear medicine diagnosis and cancer therapy.

Over the past few decades, several TfR1-targeted imaging agents have been developed. One of the oldest examples is [^{67}Ga]Ga-citrate [11-13]. Although its uptake mechanism in tumor tissues is not fully understood, it is believed that gallium ions form a stable complex with transferrin in the serum and are subsequently taken up by TfR1. However, the broad application of [^{67}Ga]Ga-citrate for TfR1 imaging is hampered by several drawbacks, such as low tumor-to-background ratios, prolonged waiting times (2-3 days) between injection and image acquisition, and unclear tumor accumulation mechanisms. Transferrin, a glycoprotein with a MW of 77-80 kDa, is an endogenous ligand of TfR1. Therefore, radiolabeled transferrin derivatives have been considered TfR1-targeted imaging agents [14-16]. However, they also suffer from the same issues of low tumor-to-background ratios and prolonged waiting times between the injection and image acquisition as [^{67}Ga]Ga-citrate. Radiolabeled monoclonal antibodies are another class of TfR1 imaging agents with high affinity and selectivity. Sugyo et al. radiolabeled TSP-A01, a monoclonal antibody against TfR1, with ^{111}In and ^{89}Zr, and these radiolabeled antibodies showed high and specific accumulation in TfR1-positive tumors both in vitro and in vivo [17-19]. On the other hand, several days are needed after the injection of [^{89}Zr]Zr-TSP-A01 to obtain optimal PET images due to its slow blood clearance, which could hinder its clinical application.

Radiolabeled peptides represent another class of imaging agents characterized by rapid blood clearance, high affinity, and high specificity, and are extensively studied for their clinical applications [20]. Indeed, several radiolabeled peptides, including [^{68}Ga]Ga-DOTA-TATE, are widely used in the clinical diagnosis of cancer [21]. On the other hand, to date, only one radiolabeled peptide has been evaluated as a TfR1 imaging agent [22]. In the report, a linear peptide (THRPPMWSPVWP) was employed as a TfR1 ligand and radiolabeled with ^{68}Ga. In vitro cellular uptake experiments indicated that the ^{68}Ga-labeled peptide accumulated nonspecifically in TfR1-positive cell lines, due to its insufficient binding affinity to TfR1. While several other linear peptides have been identified as potential TfR1 binders [23, 24], none have been reported as TfR1 imaging agents. In this study, we explored cystine-dense peptides as promising ligand candidates for TfR1 imaging. Cystine-dense

peptides are a category of peptides that are characterized by the presence of several disulfide bonds in the backbone structure and could exhibit excellent affinity and specificity equivalent to those of antibodies [25-27]. Recently, Crook et al. screened a large pool of cystine-dense peptides using a novel mammalian surface display method and identified TfRB1G3 as a promising ligand for TfR1 [28]. Surprisingly, the TfR1 binding affinity of TfRB1G3 was even higher than that of holo-transferrin, the endogenous ligand for TfR1. However, the potential applicability of TfRB1G3 as a TfR1 imaging agent has not been evaluated.

In this study, we chemically introduced a chelating moiety to TfRB1G3 and radiolabeled it with ^{67}Ga for cell-based and ex vivo biodistribution experiments, and with ^{68}Ga for PET/CT imaging (Fig. 1). The potential of ^{68}Ga-labeled TfRB1G3 as a PET imaging agent for TfR1-positive tumors was evaluated through preclinical experiments.

Materials and methods

Chemistry and Radiochemistry

HBED-CC-tris(*t*Bu)ester (**1**) (*N*, *N*'-Bis[2-hydroxy-5-(carboxyethyl)-benzyl]ethylenediamine-*N*, *N*'-diacetic acid, tris *tert*-butyl ester) was purchased from ABX Advanced Biochemical Compounds Co. (Radeberg, Germany). Hexynoyl-TfRB1G3 (**4**), whose detailed chemical structure can be found in the Supplemental Information, was custom synthesized by Peptide Institute Inc. (Osaka, Japan). All other reagents were purchased from FUJIFILM Wako Pure Chemical Industries, Ltd. (Osaka, Japan), Tokyo Chemical Industry, Co., Ltd. (Tokyo, Japan), or Watanabe Chemical Industries, Ltd. (Hiroshima, Japan). Mass spectrometry was carried out using Solaris XR (Bruker Daltonics, Bremen, Germany).

The detailed synthesis procedure for HBED-CC-TfRB1G3 (**6**) can be found in the Supplemental Information (Fig. S1). For radiolabeling, 30 μL of 2.0 M HEPES (pH 4.0) buffer and 0.5 nmol of HBED-CC-TfRB1G3 (**6**) dissolved in 40 μL water were mixed, followed by the addition of 1-7 MBq / 30 μL of [^{67}Ga]$GaCl_3$ (PDRadiopharma Inc., Tokyo, Japan) in 0.1 M HCl or 10-20 MBq / 30 μL of freshly eluted [^{68}Ga]$GaCl_3$ in 0.1 M HCl from a ^{68}Ge/^{68}Ga generator (Galli Eo®, IRE-ELiT Co., Belgium) (Fig. 1). The reaction solution was left at room temperature for 10 min. After radiolabeling, [^{67}Ga]Ga-TfRB1G3 was used for subsequent experiments without post-labeling purification. [^{68}Ga]Ga-TfRB1G3 was used for the small-animal PET/CT study after purification by a PD SpinTrap G-25 desalting column (Cytiva, Japan) equilibrated with PBS. The radiochemical purity was analyzed by HPLC (LC-20AD, Shimadzu Co., Japan) with an in-line NaI(Tl) radio-detector (Gabi Star®, Elysia Raytest Co., Straubenhardt, Germany) using system 2-2 (Table S2).

Cell culture and siRNA transfection

A human glioblastoma cell line (U87MG) was obtained from ATCC (Manassas, Virginia) and cultured in a high-glucose DMEM supplemented with 10% v/v fetal bovine serum (Nippon Biosupply Center, Tokyo, Japan) and 1% v/v penicillin–streptomycin (10,000 unit-10 mg/mL, FUJIFILM Wako Pure Chemical Industries, Ltd. Osaka, Japan) at 37 °C in humidified atmosphere containing 5% CO_2. U87MG cells were transfected with non-targeting siRNA (ON-TARGET plus non-targeting pool, D-001810-10-05, Dharmacon Inc., Lafayette, Colorado) or TfR1-targeting siRNA (ON-TARGET plus SMART pool Human TFRC, L-003941-00-0005, Dharmacon Inc., Lafayette, Colorado) using Lipofectamine™ RNAiMAX Transfection Reagent (Thermo Fisher Scientific Inc., Waltham, Massachusetts) following a previous report [29] and the manufacturer's protocol. The TfR1 expression levels in U87MG cells transfected with non-targeting siRNA ($U87MG^{siCont}$) and TfR1-targeting siRNA ($U87MG^{siTfR1}$) were analyzed by western blotting. The transfected cells were prepared in 24-well Type I collagen-coated plates (AGC TECHNO GLASS Co., Ltd., Shizuoka, Japan) for subsequent experiments.

In vitro cellular accumulation study of [^{67}Ga]Ga-TfRB1G3

$U87MG^{siCont.}$ and $U87MG^{siTfR1}$ were prepared according to the method described in the *Cell culture and siRNA transfection* section and were incubated with 50 μL [^{67}Ga]Ga-TfRB1G3 (10 kBq, containing 20 pmol of the precursor) and 450 μL HBSS (+) (FUJIFILM Wako Pure Chemical Industries, Ltd., Osaka, Japan) at 37°C for 1 h. Total incubation volume was 500 μL per well. After the incubation, the cells were washed three times with ice-cold PBS and lysed in 500 μL of 0.1 M NaOH. The radioactivity in the lysates was measured by a γ-counter (Wizard 2 2480, Perkin-Elmer, Waltham, Massachusetts). The protein concentration in the lysates was determined using a micro-BCA assay (Thermo Fisher Scientific Inc., Waltham, Massachusetts) with bovine serum albumin (BSA) as the protein standard. The radioactivity in the lysates was normalized to the protein content and expressed as %Dose/mg protein, representing the total cellular accumulation. This experiment was performed once with triplicate samples.

U87MG cells not transfected with siRNA were used for the internalization study. U87MG cells were seeded at a density of 1×10^5 cells per well in 24-well Type I collagen-coated plates and incubated overnight. The cells were incubated with [^{67}Ga]Ga-TfRB1G3 (10 kBq, containing 20 pmol of the precursor in 500 μL medium in each well) in HBSS (+) at 37 °C or 4 °C. At 5, 10, 30, and 60 min after incubation, the cells were washed three times with ice-cold PBS and then treated with 500 μL of 0.2 M glycine buffer (pH 2.5) for 1 min on ice. The acidic solution was collected and considered the membrane-bound fraction of [^{67}Ga]Ga-TfRB1G3. Then, the cells were lysed in 500 μL of 0.1 M NaOH, and the cell lysates were considered the internalized fraction of [^{67}Ga]Ga-TfRB1G3. The radioactivity in each fraction was reported as %Dose/mg protein. This experiment was performed once with triplicate samples.

Saturation binding study of [^{67}Ga]Ga-TfRB1G3

U87MG cells not transfected with siRNA were used for the saturation binding study. U87MG cells were seeded as described elsewhere and were incubated with increasing concentrations of [^{67}Ga]Ga-TfRB1G3 (20 pM to 100 nM) in HBSS (+) at 4°C for 1 h. The cells were washed three times with ice-cold PBS and lysed in 500 μL of 0.1 M NaOH. The radioactivity and protein concentration of the lysates were measured as described elsewhere. The dissociation constant (K_D) and maximum binding sites (Bmax) values were calculated from a nonlinear regression curve fitting to the experimental data using GraphPad Prism v.7 (GraphPad Software, Inc., San Diego, California). This experiment was performed once with triplicate samples.

Animal model

BALB/c mice and BALB/c nu/nu nude mice were purchased from Japan SLC (Hamamatsu, Japan). All animal experiments were performed following the Guidelines of the Institutional Animal Care and Use Committee of Hokkaido University and were approved by the Institutional Animal Care and Use Committee (Approval Number: 19-0150). U87MG cells (5×10^6 cells / 50 μL of DMEM) were inoculated subcutaneously into the left forelimbs of five-week-old male BALB/c nu/nu nude mice under anesthesia induced with 2% isoflurane (Pifzer, Tokyo, Japan). Mice were subjected to either the PET/CT experiment or the ex vivo biodistribution experiment when the tumor volumes reached 200–500 mm^3.

Ex vivo biodistribution study of [^{67}Ga]Ga-TfRB1G3

Five-week-old male BALB/c normal mice were injected intravenously with 100 μL of [^{67}Ga]Ga-TfRB1G3 (10 kBq, 20 pmol of the precursor) in PBS. At 30, 60, and 120 min after injection, the mice were sacrificed, and blood samples and organs of interest were collected and weighed. Their radioactivity was measured by a γ-counter. Biodistribution results were expressed as %ID/g. Seven-week-old male BALB/c-nu/nu mice bearing U87MG tumors were divided into non-blocking and blocking groups (n = 3-4) and were injected intravenously with 100 μL of [^{67}Ga]Ga-TfRB1G3 (10 kBq, containing 20 pmol of the precursor) in PBS. The mice were sacrificed at 60 min after injection, and the biodistribution results were analyzed as described above. To the blocking group, 10 nmol of TfRB1G3 was co-injected.

Small-animal PET/CT imaging study of [^{68}Ga]Ga-TfRB1G3

Eight-week-old male BALB/c-nu/nu mice bearing U87MG tumors were injected intravenously with 100 μL of [^{68}Ga]Ga-TfRB1G3 (3.7-7.4 MBq, containing 0.5 nmol of the precursor) in PBS. To the blocking group, 10 nmol of TfRB1G3 was co-injected. The mice were anesthetized with 4% (v/v) isoflurane and maintained under 1% (v/v) isoflurane. They were positioned on the imaging bed for micro-PET/CT imaging (Inveon, Siemens Healthineers Inc., Erlangen, Germany) using list-mode acquisitions. Whole-body PET images at 20 (15-25), 50 (45-55), and 110 (105-115) min after the

injection were reconstructed and corrected for attenuation and scatter using 3D-OSEM with CT-based attenuation correction. Regions of interest (ROIs) were drawn on the CT images and further mapped onto the PET images. The radioactivity in each ROI was quantified as the SUVmean using Inveon Workplace software (Siemens Healthineers Inc., Erlangen, Germany).

Statistical analysis-

All results are expressed as the mean ± S.D. Statistical significance was calculated with unpaired Student's *t* tests in GraphPad Prism 7.

Results

Synthesis and Radiochemistry

[^{67}Ga]Ga-TfRB1G3 was obtained with 95.0 ± 0.9% radiochemical purity without post-labeling purification. Thus, it was directly used in cell-based and ex vivo biodistribution experiments. In contrast, [^{68}Ga]Ga-TfRB1G3 required purification via gel filtration following the radiolabeling reaction. This purification was necessary to remove free [^{68}Ga]gallium ion and to exchange the high-concentration HEPES buffer with PBS. The activity yield, also referred to as non-decay-corrected radiochemical yield, of [^{68}Ga]Ga-TfRB1G3 was 67.9 ± 3.7%. Notably, the proportion of unchelated radiogallium was higher in the ^{68}Ga labeling reaction (~20%) compared to the ^{67}Ga reaction (<5%), despite identical labeling conditions. Although previous analyses indicated minimal metal ion contamination in the eluate of the ^{68}Ge/^{68}Ga generator used in this study [30], the potential influence of trace contaminants on labeling efficiency cannot be excluded. Following purification, the radiochemical purity of [^{68}Ga]Ga-TfRB1G3 exceeded 90%. The molar activity of [^{67}Ga]Ga-TfRB1G3 and [^{68}Ga]Ga-TfRB1G3 was 2.0-2.6 MBq/nmol and 14.0-18.8 MBq/nmol, respectively.

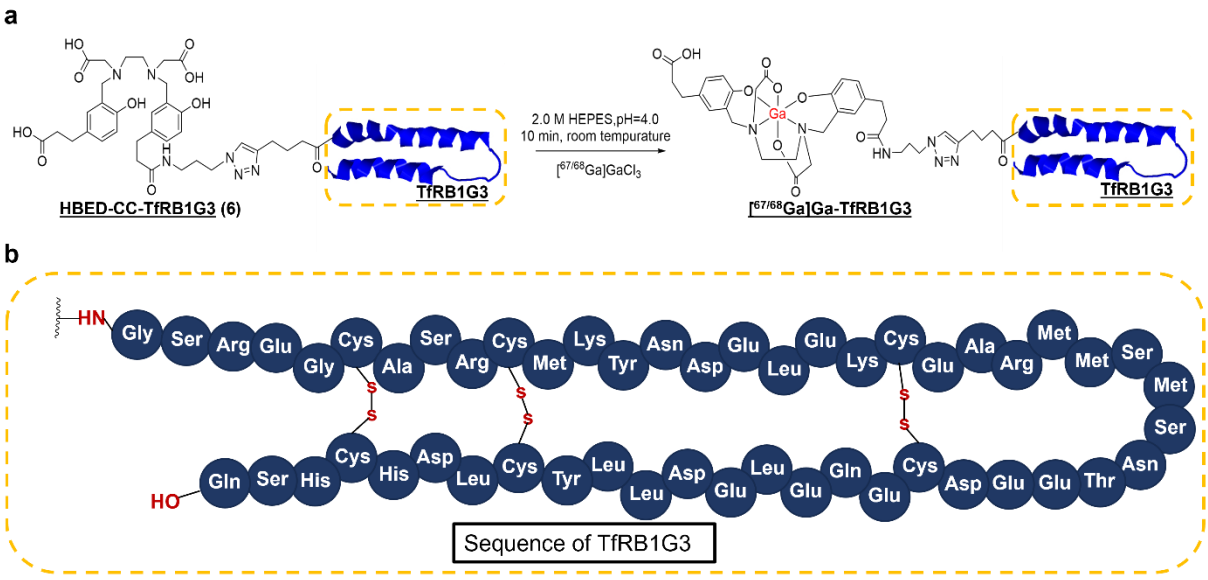

Fig. 1 (**a**) Synthetic route of [$^{67/68}$Ga]Ga-TfRB1G3 and (**b**) Structure of TfRB1G3 peptide

In vitro cellular accumulation of [^{67}Ga]Ga-TfRB1G3

The TfR1 expression levels in U87MG$^{siCont.}$ and U87MG ^{siTfR1} were shown in Fig. 2a. siTfR1 transfection reduced the TfR1 expression level by over 90%, which indicated the successful knockdown of TfR1 in U87MG^{siTfR1}. The TfR1-specific accumulation of [^{67}Ga]Ga-TfRB1G3 was evaluated by comparing its accumulation in U87MG$^{siCont.}$ and U87MG^{siTfR1}. As shown in Fig. 2b, the accumulation of [^{67}Ga]Ga-TfRB1G3 in U87MG^{siTfR1} (22.0 ± 1.1% Dose/mg) was significantly lower than that in U87MG^{siCont} (308.5 ± 14.3% Dose/mg), demonstrating the remarkable specificity of [^{67}Ga]Ga-TfRB1G3 for TfR1.

The internalization efficiency of [^{67}Ga]Ga-TfRB1G3 was evaluated by an acid wash technique (Fig. 2c). At 37°C, the internalized radioactivity was much higher than the membrane-bound radioactivity. In contrast, the opposite result was obtained at 4°C. These results indicate the substantial internalization ability of [^{67}Ga]Ga-TfRB1G3 in physiological conditions.

Results of the saturation binding study are shown in Fig. 3. The K_D and B_{max} values of [^{67}Ga]Ga-TfRB1G3 to TfR1 on U87MG were 1.0 (95% confidence interval; 0.71 – 1.45) nM and 3.23×10^8 (95% confidence interval; $2.94 \times 10^8 – 3.53 \times 10^8$) receptors per mg protein, respectively.

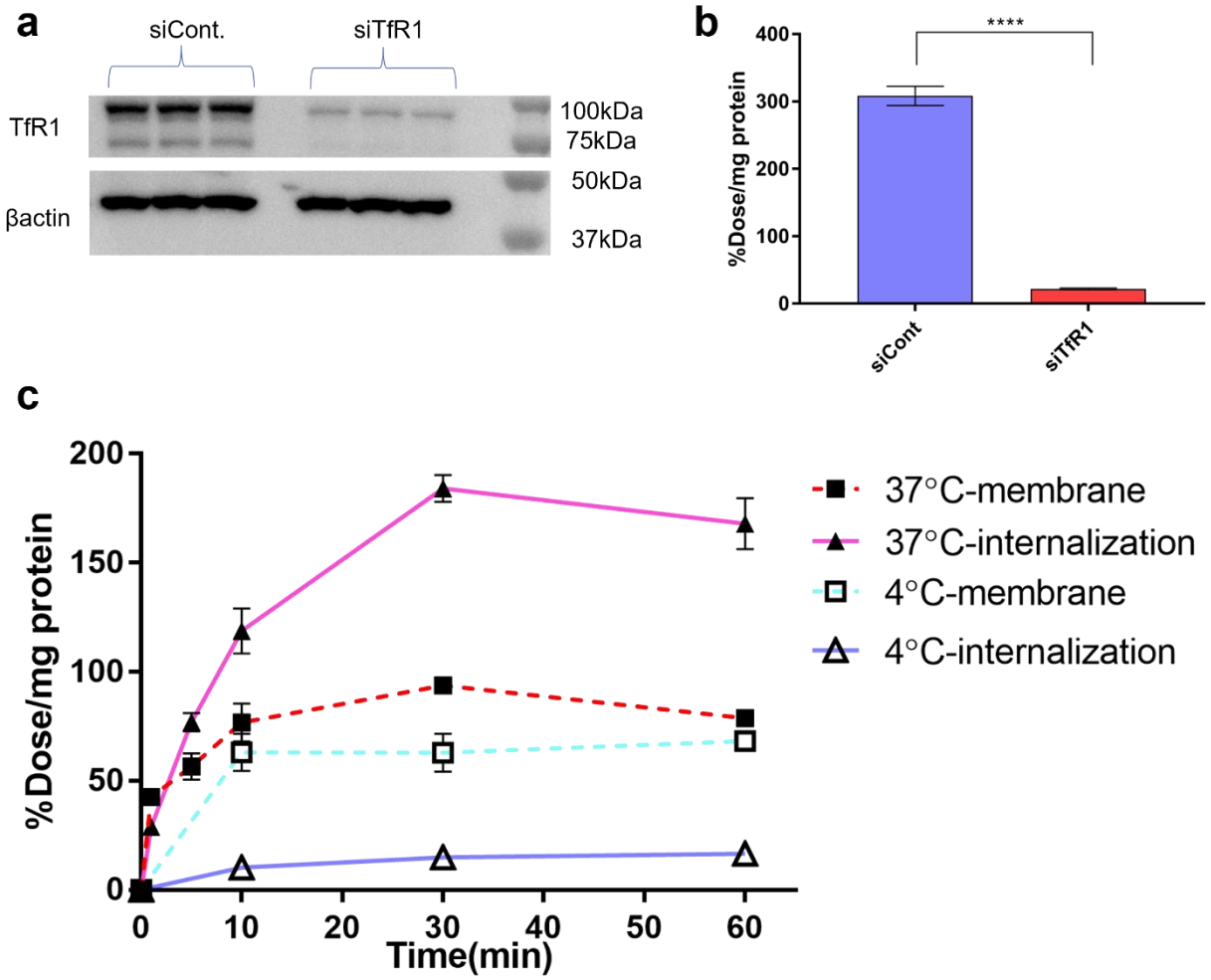

Fig. 2 Cellular accumulation studies in U87MG tumor cells. (**a**) TfR1 expression in U87MG$^{siCont.}$ and U87MG ^{siTfR1} cells (n = 3). (**b**) Cellular accumulation of [^{67}Ga]Ga-TfRB1G3 in U87MG$^{siCont.}$ and U87MG ^{siTfR1} cells after 1 h incubation at 37°C (n = 3). (**c**) Cellular internalization pattern of [^{67}Ga]Ga-TfRB1G3 in U87MG cells at 4 or 37°C (n = 3); ****, P<0.0001, by unpaired Student's t-test

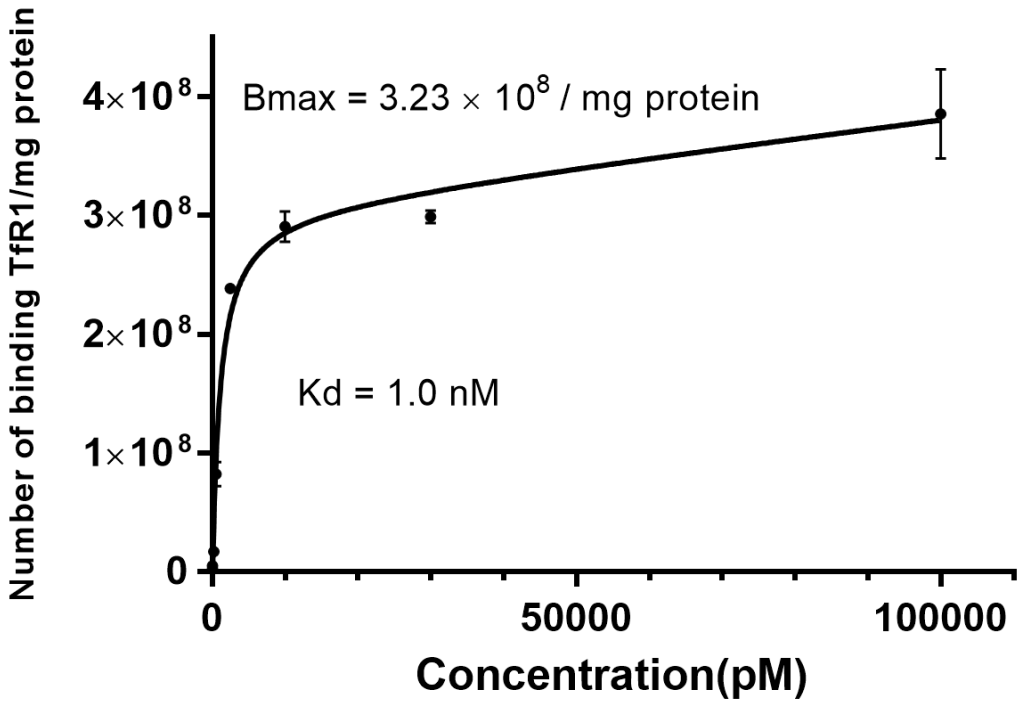

Fig. 3 Saturation binding curve ($R^2 = 0.98$) of [^{67}Ga]Ga-TfRB1G3 to TfR1 on U87MG cells at 4°C

Ex vivo biodistribution of [^{67}Ga]Ga-TfRB1G3

The ex vivo biodistribution results of [^{67}Ga]Ga-TfRB1G3 in normal mice are summarized in Fig. 4a. [^{67}Ga]Ga-TfRB1G3 was rapidly cleared from the blood pool and was excreted mainly via the kidneys and partly via the gastrointestinal tract. Although the initial renal accumulation was notably high, it decreased rapidly over time. In U87MG tumor-bearing nude mice (Fig. 4b), the tumor accumulation of [^{67}Ga]Ga-TfRB1G3 was higher than in any other organs except for the kidneys. In addition, the tumor accumulation was significantly reduced by more than 90% ($P < 0.001$) when co-injected with 10 nmol of TfRB1G3, indicating the high in vivo specificity of [^{67}Ga]Ga-TfRB1G3 to TfR1. The accumulation in several organs, such as the spleen, stomach, and small intestine, was also significantly reduced by the blocking, which may be attributed to the physiological expression of TfR1 in these organs [31, 32].

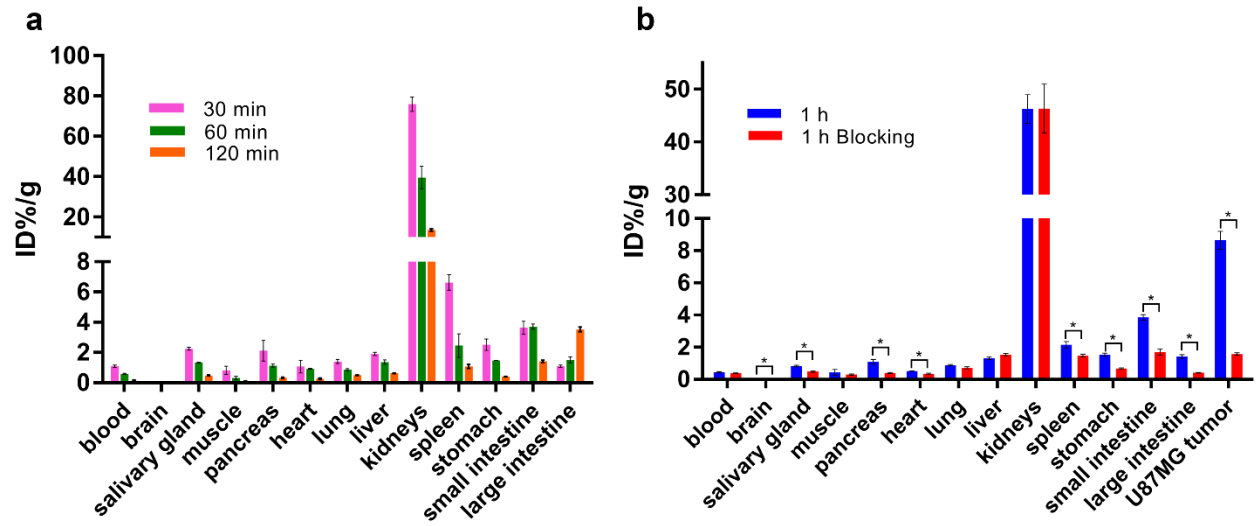

Fig. 4 (**a**) Ex vivo biodistribution of [^{67}Ga]Ga-TfRB1G3 in normal mice at 30, 60, and 120 min after injection (n = 4/group). (**b**) Ex vivo biodistribution of [^{67}Ga]Ga-TfRB1G3 in U87MG tumor-bearing nude mice at 1 h after injection, with and without co-injection of unlabeled TfRB1G3 as a blocking agent (n = 3/group); *P < 0.05, by unpaired Student's t-test

PET/CT imaging with [^{68}Ga]Ga-TfRB1G3

Representative maximum intensity projection images at different time points after injection of [^{68}Ga]Ga-TfRB1G3 are shown in Fig. 5a. The U87MG tumor was clearly visualized in the PET image as early as 20 min post-injection. The tumor accumulation was sustained throughout the 110 min imaging duration post-injection, while the accumulation in the muscle and kidneys gradually decreased, resulting in higher tumor-to-background ratios at later time points (Figs. 5b and 5c). The high TfR1 specificity of [^{68}Ga]Ga-TfRB1G3 was confirmed by the blocking experiment in which 10 nmol of TfRB1G3 was co-administered (Fig. 5a).

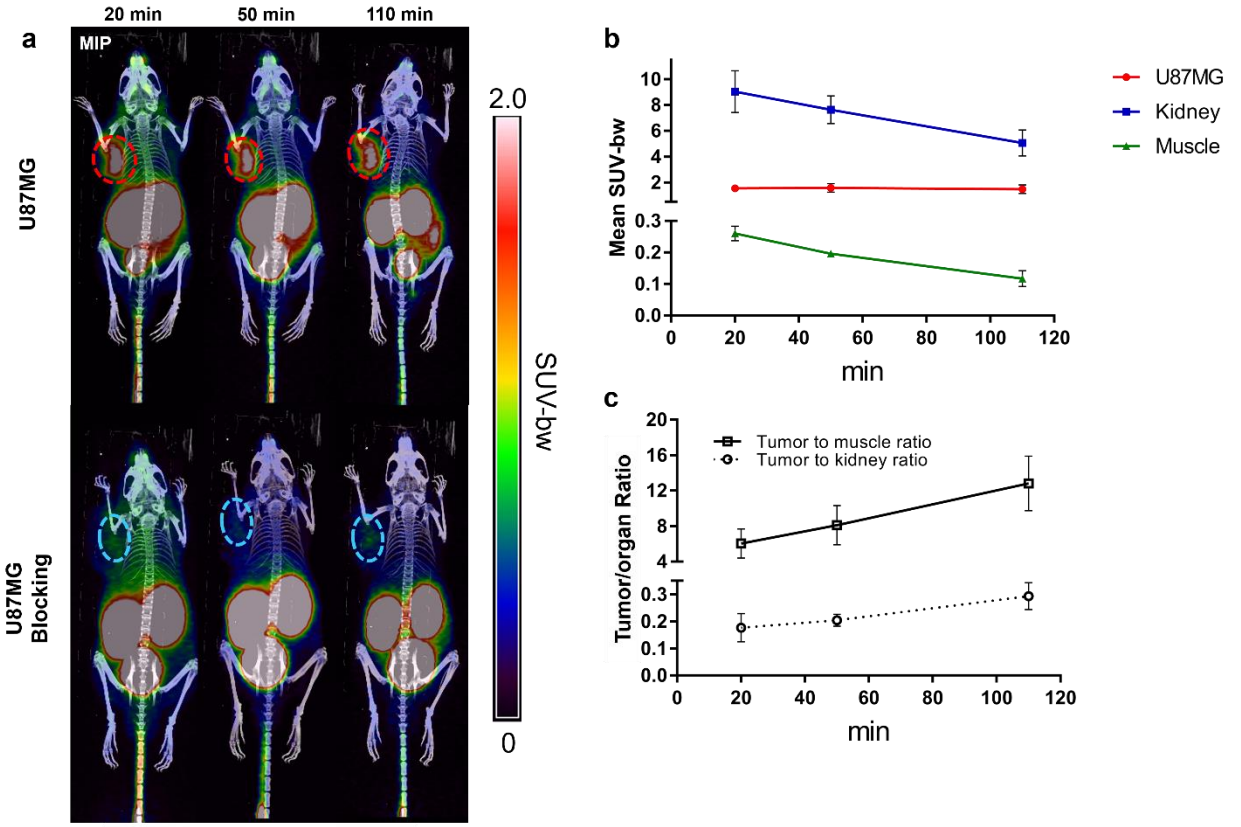

Fig. 5 Representative PET images of [^{68}Ga]Ga-TfRB1G3 accumulation in mice bearing U87MG xenografts. (**a**) Micro PET imaging of [^{68}Ga]Ga-TfRB1G3 in U87MG (red) and U87MG with blocking (blue) group. (b) The quantification results were calculated from the PET images for the U87MG tumors, kidneys, and muscle (n = 4). (**c**) The tumor-to-kidney and tumor-to-muscle ratios were calculated from the PET images (n = 4)

Discussion

In this study, we designed and synthesized [$^{67/68}$Ga]Ga-TfRB1G3, a novel peptide-based imaging agent targeting TfR1. In addition, we demonstrated that [$^{67/68}$Ga]Ga-TfRB1G3 accumulated in tumors with high affinity and specificity for TfR1. From the results of PET scans, [^{68}Ga]Ga-TfRB1G3 provided clear PET images of TfR1-positive tumors as early as 20 min post-injection with a favorable tumor-to-background ratio. PET imaging with [^{68}Ga]Ga-TfRB1G3 would enable sensitive and quantitative monitoring of TfR1 expression in vivo.

In vitro cell-based assays demonstrated that [^{67}Ga]Ga-TfRB1G3 accumulated in TfR1^{+} U87MG cells. Notably, this accumulation was reduced by more than 95% following TfR1 knockdown, confirming the high specificity of [^{67}Ga]Ga-TfRB1G3 for TfR1 (Fig. 2b). At 37 °C, most of the [^{67}Ga]Ga-TfRB1G3 was initially associated with the cell membrane and subsequently internalized. In contrast, at 4°C, it remained predominantly membrane-bound, consistent with the behavior of endogenous transferrin [33, 34]. We also conducted a saturation binding study to determine the dissociation constant and the maximum number of the binding sites (Fig. 3). The Kd (1.0 nM) and Bmax (3.23×10^{8}) for [^{67}Ga]Ga-TfRB1G3 suggest that [^{67}Ga]Ga-TfRB1G3 has high affinity to TfR1^{+} tumor cells with a significant number of available binding sites.

In vivo biodistribution and PET imaging studies demonstrated a high accumulation of [$^{67/68}$Ga]Ga-TfRB1G3 in TfR1-expressing tumor xenografts (Figs. 4 and 5). This tumor accumulation was effectively blocked by the co-injection of an excess of unlabeled TfRB1G3, providing compelling evidence of in vivo specificity for TfR1. Compared with [^{67}Ga]Ga-citrate [11-13], [^{68}Ga]Ga-TfRB1G3 exhibited superior specificity for TfR1 and more rapid blood clearance, which led to enhanced tumor accumulation in TfR1-positive tumors and enabled earlier imaging. Regarding radiolabeled transferrin, no significant difference in accumulation was observed between tumor and normal tissues for ^{68}Ga-labeled transferrin at early time points post-injection, as reported in our previous study [16]. In contrast, [^{68}Ga]Ga-TfRB1G3 achieved markedly higher tumor accumulation with an improved tumor-to-background ratio at earlier time points, such as 20 min post-injection. Although transferrin labeled with long-lived radionuclides, including ^{89}Zr[14, 15], can detect TfR1-positive tumors in vivo, imaging typically requires at least 48 hours post-injection. Similarly, antibody-based imaging agents, such as [^{89}Zr]Zr-TSP-A01[17], require 2-3 days for image acquisition due to their slow systemic clearance. Accordingly, [^{68}Ga]Ga-TfRB1G3 offers a substantial advantage over both transferrin- and antibody-based imaging agents, which require prolonged intervals between injection and imaging. To the best of our knowledge, [^{68}Ga]Ga-TfRB1G3 is the first TfR1-targeted imaging agent capable of visualizing TfR1 expression in vivo at such an early time point post-injection.

Despite these promising results, several limitations remain. First, the current study focused on a single

glioma model, thereby limiting its assessment to tumor types with variable TfR1 expression levels. Although TfR1 is overexpressed in many cancers, using only one tumor model precludes direct comparisons of [^{68}Ga]Ga-TfRB1G3 accumulation across different malignancies. Nonetheless, this work represents the first preclinical evaluation of this novel radiopharmaceutical, demonstrating its potential by assessing cellular accumulation, biodistribution, and optimal imaging time points after probe injection. Particularly, the favorable results, showing higher accumulation of [^{68}Ga]Ga-TfRB1G3 in tumors than in any other organ except the kidneys (Figs. 4 and 5), suggest that it has potential for various tumor imaging applications and warrant further investigation. Second, this study employed a subcutaneous xenograft model of glioma, which does not fully replicate the clinical characteristic of glioma in patients. As shown in Fig. 4, the accumulation of [^{67}Ga]Ga-TfRB1G3 in the brain was substantially low, indicating that this radioligand does not efficiently cross the intact blood brain barrier. Consequently, the accumulation of [^{68}Ga]Ga-TfRB1G3 in glioma tissues may be limited when the blood brain barrier remains intact. However, it is important to note that the integrity of the blood brain barrier is often compromised in glioma patients [35-37], potentially allowing [^{68}Ga]Ga-TfRB1G3 to penetrate brain tissues and bind to TfR1 expressed on glioma cells. Future studies employing orthotopic glioma models would be essential to more accurately assess the potential and limitations of [^{68}Ga]Ga-TfRB1G3 for imaging glioma in a clinically relevant context. Finally, the renal accumulation of [^{68}Ga]Ga-TfRB1G3 remains relatively high. Future optimization of its pharmacokinetics may be achieved by incorporating cleavable linkers between the chelator and peptide [38, 39] , which represents a key direction for further enhancing its clinical value.

Because of the overexpression of TfR1 in many types of tumor cells, efforts have been made to develop TfR1-targeted cancer therapies [40, 41]. For the successful clinical implementation of TfR1-targeted therapies, it is crucial to select patients with TfR1-positive tumors who are likely to benefit from the treatment. [^{68}Ga]Ga-TfRB1G3 PET imaging would enable the selection of such patients by providing a non-invasive evaluation of TfR1 expression in tumor tissues. This is a significant advantage over other invasive diagnostic methods, such as biopsy, which requires tissue sampling to assess TfR1 expression. Another advantage is associated with the rapid pharmacokinetics of [^{68}Ga]Ga-TfRB1G3, which are clinically beneficial in reducing patient burden and radiation exposure. Additionally, ^{68}Ga is one of the most clinically accessible PET radionuclides due to the availability of commercially produced ^{68}Ge/^{68}Ga generators. The short physical half-life of ^{68}Ga allows re-examination as early as the following day, which makes it possible to monitor dynamic changes in TfR1 expression levels. Furthermore, HBED-CC-TfRB1G3, the precursor of [^{68}Ga]Ga-TfRB1G3, can be chemically synthesized. This feature can potentially reduce production costs and offer an additional advantage over protein-based imaging agents, which are typically produced by bacteria or mammalian cells, followed by complex purification processes. Thus, [^{68}Ga]Ga-TfRB1G3 has the potential to serve as a clinically useful companion diagnostic agent to TfR1-targeted cancer therapies. TfR1 also plays an important role in ferroptosis [42], a form of regulated cell death characterized by

intracellular iron overload and lipid peroxidation. Due to its distinctive mechanism from other forms of cell death, effective ferroptosis inducers are expected to be promising drug candidates for cancer therapy [41, 43]. Our group recently reported that the TfR1 expression level, as determined by radiolabeled transferrin, may predict the sensitivity of cancer cells to a ferroptosis inducer [16]. In addition, it has also been demonstrated that the TfR1 expression level is upregulated upon the induction of ferroptosis [29], though the exact mechanism remains to be elucidated. Thus, in vivo imaging of TfR1 using [^{68}Ga]Ga-TfRB1G3 may serve as a valuable tool in ferroptosis research, including prediction of treatment sensitivity, assessment of early response to ferroptosis induction, and understanding of the role of TfR1 in ferroptosis progression.

Notably, the tumor accumulation of [^{68}Ga]Ga-TfRB1G3 did not decrease over the whole imaging period, while the renal accumulation gradually decreased during the same period (Fig. 5b). This result suggests that TfRB1G3, radiolabeled with a therapeutic radionuclide possessing a longer physical half-life, can be used for targeted radiopharmaceutical therapy, as the radiation dose to the tumor expected to be higher than that to the kidneys. Although TfRB1G3 derivatives labeled with another radionuclide may exhibit different pharmacokinetic profiles, the potential of TfRB1G3 for TfR1-targeted radiopharmaceutical therapy deserves further evaluation.

Conclusion

In this study, we designed and synthesized [^{68}Ga]Ga-TfRB1G3, a novel peptide-based PET imaging agent targeting TfR1, and evaluated its potential through preclinical experiments. [^{68}Ga]Ga-TfRB1G3 showed excellent affinity and specificity for TfR1. [^{68}Ga]Ga-TfRB1G3 provided clear PET images of TfR1-positive tumors shortly after the injection, a significant advantage over protein-based TfR1 imaging agents. In vivo imaging of TfR1 using [^{68}Ga]Ga-TfRB1G3 offers various potential applications, which include assessing the prognosis of cancer patients, selecting eligible patients for TfR1-targeted therapy, and elucidating the role of TfR1 in ferroptosis. Thus, [^{68}Ga]Ga-TfRB1G3 would make a significant contribution to both clinical and fundamental research involving TfR1.

REFERENCES

1. Bennett MJ, Lebrón JA, Bjorkman PJ. Crystal structure of the hereditary haemochromatosis protein HFE complexed with transferrin receptor. Nature. 2000;403:46-53. doi:10.1038/47417.

2. Cheng Y, Zak O, Aisen P, Harrison SC, Walz T. Structure of the Human Transferrin Receptor-Transferrin Complex. Cell. 2004;116:565-76. doi:10.1016/s0092-8674(04)00130-8.

3. Shaul YD, Yuan B, Thiru P, Nutter-Upham A, Mccallum S, Lanzkron C, et al. MERAV: a tool for comparing gene expression across human tissues and cell types. Nucleic Acids Research. 2016;44:D560-D6. doi:10.1093/nar/gkv1337.

4. Thul PJ, Lindskog C. The human protein atlas: A spatial map of the human proteome. Protein Science. 2018;27:233-44. doi:10.1002/pro.3307.

5. Shen Y, Li X, Dong DD, Zhang B, Xue YR, Shang P. Transferrin receptor 1 in cancer: a new sight for cancer therapy. American Journal of Cancer Research. 2018;8:916-31.

6. Zhang D, Duque-Jimenez J, Facchinetti F, Brixi G, Rhee K, Feng WW, et al. Transferrin receptor targeting chimeras for membrane protein degradation. Nature. 2024. doi:10.1038/s41586-024-07947-3.

7. Kim H, Villareal LB, Liu Z, Haneef M, Falcon DM, Martin DR, et al. Transferrin Receptor-Mediated Iron Uptake Promotes Colon Tumorigenesis. Adv Sci (Weinh). 2023;10:e2207693. doi:10.1002/advs.202207693.

8. Schonberg L, David, Miller E, Tyler, Wu Q, Flavahan A, William, Das K, Nupur, Hale S, James, et al. Preferential Iron Trafficking Characterizes Glioblastoma Stem-like Cells. Cancer Cell. 2015;28:441-55. doi:10.1016/j.ccell.2015.09.002.

9. Hansen FJ, Mittelstädt A, Clausen F-N, Knoedler S, Knoedler L, Klöckner S, et al. CD71 expressing circulating neutrophils serve as a novel prognostic biomarker for metastatic spread and reduced outcome in pancreatic ductal adenocarcinoma patients. Scientific Reports. 2024;14. doi:10.1038/s41598-024-70916-3.

10. O'Donnell KA, Yu D, Zeller KI, Kim JW, Racke F, Thomas-Tikhonenko A, et al. Activation of transferrin receptor 1 by c-Myc enhances cellular proliferation and tumorigenesis. Mol Cell Biol. 2006;26:2373-86. doi:10.1128/MCB.26.6.2373-2386.2006.

11. Sohn MH, Jones BJ, Whiting JH, Datz FL, Lynch RE, Morton KA. Distribution of gallium-67 in normal and hypotransferrinemic tumor-bearing mice. J Nucl Med. 1993;34:2135-43.

12. Weiner RE. The mechanism of 67Ga localization in malignant disease. Nucl Med Biol. 1996;23:745-51. doi:10.1016/0969-8051(96)00119-9.

13. Even-Sapir E, Israel O. Gallium-67 scintigraphy: a cornerstone in functional imaging of lymphoma. Eur J Nucl Med Mol Imaging. 2003;30 Suppl 1:S65-81. doi:10.1007/s00259-003-1164-7.

14. Holland JP, Evans MJ, Rice SL, Wongvipat J, Sawyers CL, Lewis JS. Annotating MYC status with 89Zr-transferrin imaging. Nat Med. 2012;18:1586-91. doi:10.1038/nm.2935.

15. Henry KE, Dilling TR, Abdel-Atti D, Edwards KJ, Evans MJ, Lewis JS. Noninvasive

1 ⁸⁹Zr-Transferrin PET Shows Improved Tumor Targeting Compared with
2 ¹⁸F-FDG PET in MYC-Overexpressing Human Triple-Negative Breast Cancer. Journal
3 of Nuclear Medicine. 2018;59:51-7. doi:10.2967/jnumed.117.192286.
4 16. Shibata Y, Yasui H, Higashikawa K, Kuge Y. Transferrin-based radiolabeled probe predicts the
5 sensitivity of human renal cancer cell lines to ferroptosis inducer erastin. Biochem Biophys Rep.
6 2021;26:100957. doi:10.1016/j.bbrep.2021.100957.
7 17. Sugyo A, Tsuji AB, Sudo H, Nagatsu K, Koizumi M, Ukai Y, et al. Preclinical evaluation of ^{89}Zr-
8 labeled human antitransferrin receptor monoclonal antibody as a PET probe using a pancreatic cancer
9 mouse model. Nucl Med Commun. 2015;36:286-94. doi:10.1097/MNM.0000000000000245.
10 18. Sugyo A, Tsuji AB, Sudo H, Nomura F, Satoh H, Koizumi M, et al. Uptake of 111In-labeled
11 fully human monoclonal antibody TSP-A18 reflects transferrin receptor expression in normal organs
12 and tissues of mice. Oncol Rep. 2017;37:1529-36. doi:10.3892/or.2017.5412.
13 19. Sugyo A, Tsuji AB, Sudo H, Okada M, Koizumi M, Satoh H, et al. Evaluation of Efficacy of
14 Radioimmunotherapy with 90Y-Labeled Fully Human Anti-Transferrin Receptor Monoclonal
15 Antibody in Pancreatic Cancer Mouse Models. PLoS One. 2015;10:e0123761.
16 doi:10.1371/journal.pone.0123761.
17 20. Fani M, Maecke HR. Radiopharmaceutical development of radiolabelled peptides. European
18 Journal of Nuclear Medicine and Molecular Imaging. 2012;39:11-30. doi:10.1007/s00259-011-2001-
19 z.
20 21. Deppen SA, Liu E, Blume JD, Clanton J, Shi C, Jones-Jackson LB, et al. Safety and Efficacy of
21 68Ga-DOTATATE PET/CT for Diagnosis, Staging, and Treatment Management of Neuroendocrine
22 Tumors. J Nucl Med. 2016;57:708-14. doi:10.2967/jnumed.115.163865.
23 22. Wängler C, Nada D, Höfner G, Maschauer S, Wängler B, Schneider S, et al. In vitro and initial
24 in vivo evaluation of (68)Ga-labeled transferrin receptor (TfR) binding peptides as potential carriers
25 for enhanced drug transport into TfR expressing cells. Mol Imaging Biol. 2011;13:332-41.
26 doi:10.1007/s11307-010-0329-6.
27 23. Lee JH, Engler JA, Collawn JF, Moore BA. Receptor mediated uptake of peptides that bind the
28 human transferrin receptor. Eur J Biochem. 2001;268:2004-12. doi:10.1046/j.1432-
29 1327.2001.02073.x.
30 24. Tang J, Wang Q, Yu Q, Qiu Y, Mei L, Wan D, et al. A stabilized retro-inverso peptide ligand of
31 transferrin receptor for enhanced liposome-based hepatocellular carcinoma-targeted drug delivery.
32 Acta Biomater. 2019;83:379-89. doi:10.1016/j.actbio.2018.11.002.
33 25. Correnti CE, Gewe MM, Mehlin C, Bandaranayake AD, Johnsen WA, Rupert PB, et al.
34 Screening, large-scale production and structure-based classification of cystine-dense peptides. Nat
35 Struct Mol Biol. 2018;25:270-8. doi:10.1038/s41594-018-0033-9.
36 26. Herzig V, King GF. The Cystine Knot Is Responsible for the Exceptional Stability of the
37 Insecticidal Spider Toxin ω-Hexatoxin-Hv1a. Toxins (Basel). 2015;7:4366-80.
38 doi:10.3390/toxins7104366.

27. Kikuchi K, Sugiura M, Kimura T. High Proteolytic Resistance of Spider-Derived Inhibitor Cystine Knots. Int J Pept. 2015;2015:537508. doi:10.1155/2015/537508.
28. Crook ZR, Girard E, Sevilla GP, Merrill M, Friend D, Rupert PB, et al. A TfR-Binding Cystine-Dense Peptide Promotes Blood-Brain Barrier Penetration of Bioactive Molecules. J Mol Biol. 2020;432:3989-4009. doi:10.1016/j.jmb.2020.04.002.
29. Feng H, Schorpp K, Jin J, Yozwiak CE, Hoffstrom BG, Decker AM, et al. Transferrin Receptor Is a Specific Ferroptosis Marker. Cell Reports. 2020;30:3411-23.e7. doi:10.1016/j.celrep.2020.02.049.
30. Tomita S, Higashikawa, K., Ueno, S., Mizuno, Y., Tazawa, S., & Kuge, Y. Long-term Quality Control Test of a ^{68}Ge/68Ga Generator. *Kaku igaku The Japanese journal of nuclear medicine*. 2021;*58*:47–58. doi:10.18893/kakuigaku.tr.2102.
31. Gatter KC, Brown G, Trowbridge IS, Woolston RE, Mason DY. Transferrin receptors in human tissues: their distribution and possible clinical relevance. Journal of Clinical Pathology. 1983;36:539-45. doi:10.1136/jcp.36.5.539.
32. Daniels TR, Delgado T, Rodriguez JA, Helguera G, Penichet ML. The transferrin receptor part I: Biology and targeting with cytotoxic antibodies for the treatment of cancer. Clin Immunol. 2006;121:144-58. doi:10.1016/j.clim.2006.06.010.
33. Hopkins CR, Trowbridge IS. Internalization and processing of transferrin and the transferrin receptor in human carcinoma A431 cells. J Cell Biol. 1983;97:508-21. doi:10.1083/jcb.97.2.508.
34. Azizi F, Wahl P. Fluorescence recovery after photobleaching (FRAP) of a fluorescent transferrin internalized in the late transferrin endocytic compartment of living A431 cells: experiments. Biochim Biophys Acta. 1997;1327:75-88. doi:10.1016/s0005-2736(97)00046-1.
35. Kawauchi D, Narita Y. The curse of blood–brain barrier and blood–tumor barrier in malignant brain tumor treatment. International Journal of Clinical Oncology. 2025;30:1276-86. doi:10.1007/s10147-025-02777-3.
36. Pruis IJ, Van Dis V, Maas SLN, Balvers RK, Van Den Bosch TPP, Segbers M, et al. PSMA radioligand uptake correlates with PSMA expression in high-grade glioma and brain metastasis: insights from a prospective PET-MRI guided multiregional biopsy study. European Journal of Nuclear Medicine and Molecular Imaging. 2025. doi:10.1007/s00259-025-07338-4.
37. Mathew-Schmitt S, Peindl M, Neundorf P, Dandekar G, Metzger M, Nickl V, et al. Blood-tumor barrier in focus - investigation of glioblastoma-induced effects on the blood-brain barrier. Journal of Neuro-Oncology. 2024;170:67-77. doi:10.1007/s11060-024-04760-w.
38. Uehara T, Yokoyama M, Suzuki H, Hanaoka H, Arano Y. A Gallium-67/68–Labeled Antibody Fragment for Immuno-SPECT/PET Shows Low Renal Radioactivity Without Loss of Tumor Uptake. Clinical Cancer Research. 2018;24:3309-16. doi:10.1158/1078-0432.ccr-18-0123.
39. Zhang M, Kang F, Xing T, Wang J, Ma T, Li G, et al. First-in-human validation of enzymolysis clearance strategy for decreasing renal radioactivity using modified [68Ga]Ga-HER2 Affibody. European Journal of Nuclear Medicine and Molecular Imaging. 2024;51:1713-24. doi:10.1007/s00259-023-06584-8.

40. Candelaria PV, Leoh LS, Penichet ML, Daniels-Wells TR. Antibodies Targeting the Transferrin Receptor 1 (TfR1) as Direct Anti-cancer Agents. Front Immunol. 2021;12:607692. doi:10.3389/fimmu.2021.607692.
41. Daniels TR, Delgado T, Helguera G, Penichet ML. The transferrin receptor part II: targeted delivery of therapeutic agents into cancer cells. Clin Immunol. 2006;121:159-76. doi:10.1016/j.clim.2006.06.006.
42. Dixon J, Scott, Lemberg M, Kathryn, Lamprecht R, Michael, Skouta R, Zaitsev M, Eleina, Gleason E, Caroline, et al. Ferroptosis: An Iron-Dependent Form of Nonapoptotic Cell Death. Cell. 2012;149:1060-72. doi:10.1016/j.cell.2012.03.042.
43. Yang WS, Stockwell BR. Synthetic lethal screening identifies compounds activating iron-dependent, nonapoptotic cell death in oncogenic-RAS-harboring cancer cells. Chem Biol. 2008;15:234-45. doi:10.1016/j.chembiol.2008.02.010.

Acknowledgement

We thank ATOX Co., Ltd. for providing the $^{68}Ge/^{68}Ga$ generator used in the study. We are also deeply grateful to the staff members of the Central Institute of Isotope Science, Hokkaido University, for their skillful technical assistance.

Funding

This research was supported by JSPS KAKENHI Grant Number 21H02858 and JST SPRING, Grant Number JPMJSP2119.

Declarations

Ethical approval All animal experiments were performed following the Guidelines of the Institutional Animal Care and Use Committee of Hokkaido University and were approved by the Institutional Animal Care and Use Committee (Approval Number: 19-0150). This article does not contain any studies with human participants performed by any of the authors.

Conflict of interest The authors declare no competing interests.

Author information

Authors and Affiliations

Graduate School of Biomedical Science and Engineering, Hokkaido University, Hokkaido 060-0815, Japan.

Longxin Lin

Central Institute of Isotope Science, Hokkaido University, Hokkaido 060-0815, Japan.

Yuki Mizuno, Yuki Shibata, Yuji Kuge

Global Center for Biomedical Science and Engineering, Hokkaido University, Hokkaido 060-0815, Japan.

Yuki Mizuno, Yuji Kuge

Faculty of Veterinary Medicine, Hokkaido University, Hokkaido 060-0818, Japan

Hironobu Yasui

Contributions

LL performed experiments, curated and analyzed the data, and drafted the original article. YM contributed to the conceptualization, data curation, formal analysis, original draft conceptualization and project administration of the study. HY, and YS contributed to methodology, validation, and supervision of the study. YK contributed to conceptualization, project administration, funding acquisition and resource allocation of the study. All authors contributed to the manuscript review and editing and approved the final version of the manuscript.

Data Availability

The raw data of the results presented in this study are available from the corresponding author upon reasonable request.